Title: The biochemical properties of a novel paraoxonase-like enzyme in *Trichoderma atroviride* strain T23 involved in the degradation of 2,2-dichlorovinyl dimethyl phosphate

Running title: Characterization of an enzyme in *T. atroviride* T23

Jianan Sun [a, b], Xu Yuan [a,b], Yaqian Li [a, b], Xinhua Wang [a, b], Jie Chen [a, b,#]

State Key Laboratory of Microbial Metabolism, Shanghai Jiao Tong University, Shanghai 200240, Peoples' Republic of China [a]; Key Laboratory of Urban (South) Agriculture, Ministry of Agriculture, School of Agriculture and Biology, Shanghai Jiao Tong University, Shanghai 200240, Peoples' Republic of China [b]

 # Corresponding author: 800 Dongchuan Road, Minhang District, Shanghai 200240, China. E-mail address: jiechen59@sjtu.edu.cn

Abstract:

Dichlorvos, is a broad-spectrum organophosphorus pesticide that is widely applied in the agricultural industry and considered a pollutant to fish and bees. *T. atroviride* strain T23, an efficient DDVP-degrading strain, could convert DDVP to dichloroacetic acid, 2,2-dichloroethanol and phosphoric acid through mineralization. RT-qPCR analysis showed *TaPon1*-like encoding an organophosphorus hydrolase, is continuously highly expressed in the process of degrading DDVP. *TaPon1*-like

23 contained an open reading frame of 1317 bp, and the deduced amino acid sequence
24 shared 21% homology with HuPON1, which also exhibits excellent hydrolysis of
25 organophosphate-oxons compounds. By analysis of gene knockout, we found the
26 Δ*TaPon1*-like knockout strain KO1 lost 35.6% of its DDVP-degradation capacity at 24 h,
27 but this loss of degradation activity was recovered when the gene was
28 complemented. Furthermore, the purified recombinant protein reTAPON1-LIKE,
29 could transform DDVP only to dimethyl phosphate and showed significant
30 paraoxonase activity (1028 U L^{-1}). The reTAPON1-LIKE enzyme showed a broad
31 degradation spectrum, degrading not only DDVP but also organophosphate-oxons
32 and lactone. The kinetic parameters (K_m and k_{cat}) of the purified reTAPON1-LIKE were
33 determined to be 0.23 mM and 204.3 s^{-1} for DDVP, respectively. The highest activity
34 was obtained at 35 °C, and the optimal pH was 8.5. The activity of reTAPON1-LIKE
35 was enhanced most significantly when 1.0 mM Ca^{2+} was added but declined when
36 1.0 mM Cu^{2+} was added. These results showed TAPON1-LIKE play an important role
37 for DDVP degradation in the first step by T23 and provided clue to comprehensively
38 understanding the degradation mechanism of organophosphate-oxons pesticides by
39 filamentous fungi.
40
41 **Importance:**
42
43 The large amounts of residues of organophosphate pesticides in agroecological
44 system has become a great threat to the safety of environment and humans.

45 Bioremediation in association with microbial is innovative technology having a
46 potential to alleviate such pollution problems. The genus *Trichoderma* is genetically
47 diverse with capabilities to degrade chemical pesticides among different strains with
48 agricultural significance. As a typical organophosphorus pesticide, it is one of the
49 most employed compounds of the family. Though it was classified as a highly toxic
50 pesticide by WHO due to its hazardous properties, it plays an important role in the
51 control of plant pests, food storage and homes, as well as to treat infections in
52 livestock. Therefore, we use DDVP as a model of organophosphate pesticide to study
53 the mechanism of *Trichoderma* degrading organophosphate pesticides, for the aim of
54 globally understanding molecular mechanism of enzymatic degradation of
55 organophosphate pesticides by beneficial fungi.

56

57 **Keywords:**

58 Biodegradation; Dichlorvos; *Trichoderma atroviride* strainT23; *TaPon1*-like

59

60 **Introduction**

61 Organophosphorus pesticides are some of the most widely used pesticides.
62 Dichlorvos, 2,2-dichlorovinyl dimethyl phosphate (DDVP), is a broad-spectrum
63 organophosphorus pesticide often applied to agricultural crops and forests and in
64 aquatic environments (1). DDVP, although usually viewed as a moderately toxic
65 pesticide, is a pollutant to fishes and bees. In China, the demand for DDVP was
66 estimated to be over 40,000 tons in 2007, and its usage is expected to increase since

five highly toxic organophosphate insecticides (e.g., parathion) have been banned (2). However, severe contamination may arise due to the widespread use and discharge of DDVP into the environment, and its residues can be detected in water, soil, vegetables, fruits, milk, and living organisms (3). In addition, DDVP is highly toxic to nontarget invertebrates and vertebrates, resulting in irreversible inhibition of acetylcholinesterase, which is needed for regulating the neurotransmitter acetylcholine (4). Therefore, developing a high-efficiency method to remove DDVP residues is necessary for environmental and food production safety.

Conventional methods for the removal of DDVP, such as chemical hydrolysis/oxidation (2) and photocatalytic oxidation (5), are difficult to apply to large contaminated areas and are very expensive. Biodegradation depending on microbial metabolism has become an attractive approach for removing hazardous chemicals such as organophosphate pesticides from the environment (6). Moreover, some selected microbes have the capacity to degrade DDVP (7), and these strains can usually be isolated from natural environments.

The genus *Trichoderma* has attained a unique position in the agricultural industry as a successful biocontrol agent against plant diseases, plant growth promoters and soil bioremediation (8). More importantly, *Trichoderma* spp. with multiple functions in soil remediation, such as removing heavy metals and chemical pesticide residues, particularly when applied together with hyperaccumulators, have been revealed.

Zhang et al. (9) isolated and characterized the *Trichoderma* strain TC5, which has high degradation activity against chlorpyrifos. In previous work, we reported that *T. atroviride* strain T23 has the capacity to degrade DDVP and that the key genes *hex1* (10) and *Tapdr2* (11) were associated with the tolerance of *T. atroviride* strain T23 to DDVP.

Additionally, several genes involved in the degradation of organophosphorus compounds, including *opd*, *opa*, *opdA*, and *mpd*, have been discovered and cloned from different bacterial species (12). However, there are few studies on organophosphorus pesticide degradation enzymes from fungi; for instance, the crucial enzymes and related genes responsible for organophosphate pesticide degradation in strain T23 have not been reported.

Luckily, some molecular details of the DDVP metabolic pathway in humans is known. For instance, paraoxonases from humans (HuPONs) have been confirmed to function in the degradation of DDVP (13). It was supposed that these genes might also be present in *T. atroviride*. Therefore, the function of these genes in the biodegradation of organophosphorus pesticides needs to be investigated. This study aimed to demonstrate whether *HuPon*s were present in *T. atroviride* strain T23 and what function strain T23 plays in the biodegradation of DDVP.

Results

111

112 The effects of DDVP on the growth of T23 and biodegradation

113

114 In Fig. 1A, DDVP degradation by strain T23 was observed after DDVP addition at 24 h.
115 DDVP may inhibit the growth of train T23, and especially high concentrations of
116 DDVP (≥ 400 μg mL^{-1}) were toxic to fungal growth and inhibited degradation. While
117 DDVP existed at 100-300 μg mL^{-1} concentration, there was a weak decrease in
118 biomass of strain T23. Even at DDVP concentrations up to 300 μg mL^{-1}, the
119 degradation rate reached 56.7%, which is more than the DDVP self-degradation rate.
120 Strain T23 grew rapidly when DDVP was inoculated in the first 24 hours and the
121 growth curve of strain with or without DDVP showed a similar trend (Fig. 1B).

122

123 --Fig. 1--

124

125 An assessment of morphological changes in response to DDVP (300 μg mL^{-1})
126 accumulation in strain T23 and the quantification of DDVP were performed by
127 SEM-EDS analysis. SEM analysis of mycelia was performed at 6, 24, and 72 h of
128 incubation. No peak of chlorine was detected by EDS (Fig. S1) and the adsorbate
129 concentration of DDVP detected using a GC-FPD showed no peak (data not shown),
130 ether. According to these results, degradation of DDVP by mycelial adsorption was
131 excluded and the enzymes that are strain T23 products are the primary factor
132 attributed to DDVP degradation.

133

134 DDVP metabolite identification

135

136 To clarify the DDVP degradation pathway of strain T23, the intermediate metabolites
137 produced during DDVP degradation were analyzed and identified by GC-MS. DDVP
138 with a retention time (RT) of 13.774 min (Fig. 2A) was still present in the medium
139 after five days. By comparing the extractions following derivatization of degraded
140 and non-degraded DDVP, GC-MS analysis of the samples gave three significantly
141 different peaks with RTs of 13.075, 14.115, and 21.83 min (Fig. 2A) representing
142 metabolites *tert*-butyldimethylsilyl derivative of 2,2-dichloroethanol, dimethyl
143 phosphate, and phosphoric acid, respectively. By comparing the anhydrous ethyl
144 ether extractions of degraded and non-degraded DDVP, GC-MS analysis of the
145 samples gave two significantly different peaks with RTs of 5.577 and 10.606 min (Fig.
146 2B) representing metabolites of 2,2-dichloroethanol and phosphoric acid.

147

148 Each of the six peaks was identified according to its mass spectrum and the NIST
149 library identification program. Compound E had the same retention time as the DDVP
150 standard (RT = 13.774 min). The mass spectral data also demonstrated that
151 compound E was DDVP (Fig. 2E). 2,2-dichloroethanol was identified following
152 derivatization, which yielded the *tert*-Butyldimethylsilyl derivative of
153 2,2-dichloroethanol [Cl_2CHCH_2OSi $(CH_3)_2C(CH_3)_3$, *m/z* 228]. The mass spectrum (Fig.
154 2D) of this molecule showed loss of H^+ at *m/z* 227.1, and mass of fragments at *m/z*

155 156.9 [$Cl_2CHC(O)OSiH_2$], 115.1 [*tert*-Butyldimethylsilyl], and 93.0 [$ClCH_2C(O)O$] were
156 evident. The mass spectrum of 2,2-dichloroethanol (Fig. 2H) showed a prominent
157 molecular ion at *m/z* 113.9 $[M]^+$, and the fragments included *m/z* 82.9 [Cl_2CH], 79
158 [$ClCHCH_2OH$], 49 [$ClCH_2$], 43 [C_2H_3O] and 31.1 [CH_3O]. Chemical ionization and a
159 caparison with two mass spectra (Fig. 2D & Fig. 2H) of authentic chemical confirmed
160 the identity of 2,2-dichloroethanol. The mass spectrum of the *tert*-Butyldimethylsilyl
161 derivative of dimethyl phosphate was shown in Fig. 2F. Although the molecular ion
162 ($[M]^+$, *m/z* 240) was not observed, the characteristic loss of *tert*-butyl (*m/z* 183) and a
163 loss of methyl (m/ z 225) were noted. The molecular ion ($[M]^+$, *m/z* 440) of the
164 *tert*-Butyldimethylsilyl derivative of phosphoric acid (Fig. 2G) was not observed, but a
165 characteristic loss of methyl (*m/z* 425.2) and a loss of *tert*-butyl (*m/z* 383.2) were
166 confirmed. Compound H with RT of 10.606m showed a molecular ion at *m/z* 127.9
167 $[M]^+$, which corresponds to dichloroacetic acid (Fig. 2H). The fragments included *m/z*
168 at 83.9 [Cl_2CH_2], 77 [ClCHCOH], 48 [ClCH].
169
170 --Fig. 2--
171
172 Dimethyl phosphate and dichloroacetic acid were novel metabolites only present in
173 the DDVP degradation pathway. 2,2-dichloroethanol and phosphoric acid were
174 metabolites existing in strain T23 growth process, but their content was significant
175 increase in DDVP degradation pathway. The peak indicated dichloroacetic acid
176 subsequently disappeared after ten days of incubation, indicating that these

177 metabolites were finally degraded. Potential catabolic pathway for DDVP degradation
178 by strain T23 was shown in Fig. 3C. The results of degradation experiments and
179 metabolite identification indicated that strain T23 could utilize DDVP through carbon
180 co-metabolism in Burk medium and completely mineralized DDVP. Thus, in light of its
181 broad-spectrum substrate specificities and complete mineralization of DDVP, strain
182 T23 has the potential to be applied to the removal of DDVP and its metabolite
183 residues from the environment.

184

185 Gene expression analysis of *TaPon1*-like in *T. atroviride*

186

187 Gene expression analysis using a reverse transcription quantitative polymerase chain
188 reaction (RT-qPCR) revealed a significant ($P < 0.001$) induction of *TaPon1*-like with
189 different DDVP concentrations at 24 h (Fig. 3A). In addition, expression of *TaPon1*-like
190 was strongly induced ($P < 0.001$) when T23 was exposed to 300 μg mL^{-1} DDVP. As
191 shown in Fig. 3B, the expression of *TaPon1*-like significantly reached its maximum at
192 6 h and expressed a continuously high level during DDVP degradation process at an
193 initial DDVP concentration of 300 μg mL^{-1} in liquid Burk medium.

194

195 --Fig. 3--

196

197 Cloning and sequence analysis of *TaPon1*-like

198

199 *TaPon1*-like cDNA was amplified from the *T. atroviride* strain T23 genome.
200 *TaPon1*-like was 1384 bp in length, including a 67-bp intron that encodes 438 amino
201 acid residues. A neighbor-joining phylogenetic tree was constructed based on the
202 amino acid sequence of TAPON1-LIKE and enzymes reported in GenBank, including
203 hydrolases derived from bacteria and mammals (Fig. 4), to infer evolutionary
204 relationships. A BLAST analysis showed that TAPON1-LIKE shared 10% to 21.83%
205 identity to paraoxonase, arylesterases, and lactonases.
206
207 --Fig. 4--
208
209 Further analysis showed that TAPON1-LIKE shared 21.36% to 21.83% identity with
210 HuPON1 proteins in the PDB database (PDB accession numbers 4Q1U.1.A, 3SRE.1.A,
211 4HHQ.1.A, AND 4HHO.1.A) such as the calcium-dependent lactonase that also
212 promiscuously catalyzes the hydrolysis of paraoxon.
213
214 HuPON1 is a six-blade β-propeller containing two calcium ions in a central tunnel.
215 The tunnel-buried calcium is critical for the enzyme's conformational stability, and
216 the solvent-exposed calcium residing at the bottom of the active-site cavity is needed
217 for catalysis (14). In comparison with HuPON1, the mimetic TAPON1-LIKE contained
218 Asn168, which ligates the catalytic calcium, while the Asp183-His184 dyad is vital for
219 stabilizing the catalytic calcium ion.
220

Moreover, TAPON1-LIKE was found to have a significant motif, XXXTLVDNXXXXD, which may be the direct catalytic calcium metal-binding region for activating hydrolysis of OPPs, which interact with the side chains of Asp269 and Glu53. Motifs PXXPXXIXLMD or DXXXXXXXXMYLXVVN may be another metal-binding regions for supposed catalytic calcium ion (15) (Fig. 5 and Fig. S4C).

--Fig. 5--

TaPon1-like function in DDVP degradation

To verify the function of the *TaPon1*-like gene in DDVP degradation, knockout mutants and complementation mutants were constructed. *TaPon1*-like knockout mutants were generated by replacing *TaPon1*-like with the *hygB* selection cassette by homologous recombination using ATMT (Fig. S2A). Twenty-seven hygromycin-resistant T23 colonies were obtained on selection plates containing timentin (300 μg mL^{-1}) and hygromycin (200 μg mL^{-1}). The individual transformants were subcultured on fresh selection plates, and eight hygromycin-resistant colonies were randomly selected for mutant validation to confirm that the knockout cassette was inserted at the correct position. *TaPon1*-like fragments were lost in top six deleted transformants but were observed in wild-type T23 (Fig. S2B). The flanking fragment from six transformants adjacent to the upper border demonstrated that the T-DNA insertion position of the knockout was correct (Fig. S2C). In addition, an

243 RT-PCR experiment using primers specific to the *TaPon1*-like sequence demonstrated
244 the complete loss of the *TaPon1*-like transcript in six transformants, while an
245 amplification product of the desired size was found in the WT (Fig. S2D). Southern
246 blotting (Fig. S2F) results showed *TaPon1*-like was replaced using an 800 bp fragment
247 of *hyg*B. We selected one suitable deletion transformant designated KO1. Using
248 similar methods, *TaPon1*-like complementation transformants were screened, and
249 the suitable one was designated CO1 (Fig. S3).
250
251 The DDVP degradation rates of strain T23 and related mutants were measured by
252 GC-FPD at an initial concentration of 300 μg mL^{-1} in Burk medium for 168 hours (h).
253 Strain T23 exhibited an excellent efficiency of degrading DDVP, and the degradation
254 rate value was 56% at the first 24 h (Fig. 6). CO1 presented a similar degradation rate
255 curve compared with strain T23, and meanwhile no DDVP was residual in treatment
256 by strain and CO1. KO1 declined in the DDVP biodegradation rate about 31% at 24 h
257 compared with strain T23. The self-degradation rate of DDVP is almost 3% per 24 h.
258 On the basis of between strain T23 and related mutants, *TaPon1*-like was shown to
259 be a key gene in DDVP biodegradation.
260
261 --Fig. 6--
262
263 Sun et al. (16) showed that among 110 genetically stable T-DNA transformants of *T.*
264 *atroviride* T23, one transformant, AMT-12, was confirmed by Southern blot analysis

265 to have single-copy inserts of T-DNA, had 10% greater DDVP-degradation capacity
266 than the wild type, and tolerated up to 800 μg mL^{-1} DDVP. Based on the changes in
267 fungal biomass, gene expression and the variation in the biodegradation rate, we
268 presumed that *TaPon1*-like played an important role in the DDVP degradation
269 pathway.
270
271 Heterologous expression and purification of TAPON1-LIKE
272
273 Bioinformatics predicted that the isoelectric point of TAPON1-LIKE protein was 6.64
274 (Fig. S4A and Fig. S4B). TAPON1-LIKE had one secretion signal peptide at the N
275 terminus, and there was no transmembrane domain in the protein (Fig. S4D). We
276 determined whether the TAPON1-like protein contributed to DDVP degradation by
277 determining the activity of a recombinant TAPON1-LIKE construct (with a 30-aa
278 secretion signal peptide removed and the remaining fragment of the ORF cloned into
279 pGEX-4T-1) produced by *E. coli* Origami B (DE3).
280
281 When TAPON1-LIKE was expressed in soluble form in *E. coli* Origami B (DE3) using
282 one vector, the GST-tagged (26 kDa) TAPON1-LIKE protein was predicted to appear at
283 approximately 71 kDa. According to the SDS-PAGE analyses, the purified enzyme
284 produced a single band and was designated reTAPONN1-LIKE (Fig. 7).
285
286 --Fig. 7--

287

288 The DDVP degradation products of purified reTAPON1-LIKE were evaluated by GC-MS
289 analysis. Only *tert*-butyldimethylsilyl derivative of dimethyl phosphate, with a
290 retention time of 14.106 min, was detected as a metabolite of DDVP biodegradation
291 (Fig. S5). Therefore, we confirmed that TAPON1-LIKE is the enzyme to transform
292 DDVP into dimethyl phosphate.

293

294 "PON1 activity" can be measured using substrates such as paraoxon, phenyl acetate,
295 4-nitrophenyl acetate, 5-thiobutylbutyrolactone (TBBL), and dihydrocoumarin (17),
296 and the substrates of above could be classified into three types as paraoxon, aryl
297 esters, and lactones. ReTAPON1-LIKE exhibited paraoxonase activity against DDVP
298 (1028±31 U L^{-1}) and chlorpyrifos-oxon (8198±53 U L^{-1}). The arylesterase activity
299 against p-nitrophenyl acetate and phenyl acetate was 6.16±0.02 U mL^{-1}. The
300 lactonase activity against hydrocoumarin was 10.89±0.06 U mL^{-1}.

301

302 The purified protein or plasma derived from human and rabbit sera has been
303 demonstrated to catalyze the hydrolysis of a broad range of substrates, including
304 some pesticides such as oxon, arylesters of carboxylic acids, and lactones of hydroxy
305 acids (18-20). Purified rabbit serum was injected into the tail veins of rats, increasing
306 the peak hydrolytic activity of rat serum toward paraoxon by 9-fold and increasing
307 that toward chlorpyrifos-oxon by 50-fold (21). The degradation of human
308 fresh-frozen plasma was rapid, with half-lives of 19.5 s for chlorpyrifos-oxon and 17.9

309 min for DDVP (22). Engineered HuPON1 in the *E. coli* expression system showed
310 kinetic parameters (K_m and V_{max}) of 0.121-0.317 mM and 34.7-245 U mg^{-1} protein for
311 chlorpyrifos-oxon and 0.957-3.22 mM and 3020-680 U mg^{-1} for phenyl acetate (23,
312 24). Although the arylesterase and lactonase activities of reTAPON1-LIKE were
313 decreased, we considered the superior catalytic efficiency against
314 organophosphate-oxons pesticides. Comprehensive analysis confirmed that
315 TAPON1-LIKE was considered PON-like, with superior catalytic efficiency against
316 organophosphate-oxons, particularly DDVP.
317
318 Biochemical properties of reTAPON1-LIKE
319
320 The substrate specificities of reTAPON1-LIKE were determined by examining its
321 activity against DDVP, chlorpyrifos-oxon, mevinphos, malaoxon, omethoate,
322 methamidophos, chlorpyrifos, triazophos, phenyl acetate, p-nitrophenyl acetate,
323 p-nitrophenyl butyrate, and 3,4-dihydrocoumarin (Table 1). Substrate spectrum
324 analysis revealed that reTAPON1-LIKE nonspecifically reacted with substrates and
325 that the enzyme could hydrolyze organophosphates, esters, and lactones. The most
326 suitable substrate for reTAPON1-LIKE was P=O phosphotriester group pesticides, such
327 as DDVP, chlorpyrifos-oxon, and mevinphos, with K_m values of 0.23, 0.32, and 0.44
328 mM, respectively. Dimethyl phosphate pesticides (another group of
329 organophosphates) were hydrolyzed by reTAPON1-LIKE but at low catalytic efficiency
330 ($\approx 10^3$ s^{-1} M^{-1}). However, reTAPON1-LIKE revealed no activity against methamidophos,

chlorpyrifos, and triazophos, which belong to the P=S phosphotriester group and methyl phosphate pesticides. The K_m values for ester substrates were very similar to those of HuPON1 (25). The k_{cat} values indicated that the catalytic efficiency of reTAPON1-LIKE against arylesters is determined by the carbon chain length of the acyl group. The reTAPON1-LIKE hydrolyzed 3,4-dihydrocoumarin, which is the most commonly used lactone, at a high catalytic efficiency (4.47×10^6 s^{-1} M^{-1}).

--Table 1--

Enzyme dynamics of reTAPON1-LIKE

A variety of environmental factors such as pH and temperature exert varied effects on the enzyme activity and stability (6). The reTAPON1-LIKE protein exhibited high activity to DDVP between pH 6.5 and 10.0 (more than 50% relative activity), and pH 8.5 was optimum for its activity (Fig. 8A). Serum paraoxonase 1 activity was reported to occur from pH 7 to 10.5 (25), and the ideal pH of the reaction is in the range of 8 to 8.5 (26, 27).

The reTAPON1-LIKE protein was active at 20-50 °C, with an optimum temperature of 35 °C using DDVP as substrate (Fig. 8B). An increase in temperature of 1 °C was associated with a 4.5% increase in PON1 activity when phenyl acetate was used as substrate (28). The optimum temperature of hydrolysis for paraoxon and phenyl

353 acetate ranges from 30-45 °C (29).

354

355 -Fig. 8--

356

357 The TAPON1-LIKE amino acid sequence shared identity with the sequences of the
358 metal-dependent hydrolases; therefore, it was deduced that metal ions might also
359 affect reTAPON1-LIKE enzymatic activity. As shown in Table 2,
360 ethylenediaminetetraacetic acid (EDTA) inhibited the enzymatic activity at a final
361 concentration of 1%; the result indicated that the reTAPON1-LIKE activity might be
362 that of a metal ion-dependent hydrolase.

363

364 --Table 2--

365

366 As can be seen in Table 2, incubation of Ca^{2+}, Zn^{2+}, Na^{+} and Ba^{2+} resulted in complete
367 reactivation to 589.7% ± 3.3%, 234.4% ± 5.6%, 176.5% ± 5.2%, and 151.6% ± 1.4%,
368 respectively. On the contrary, the Cu^{2+} and Co^{2+} ions had inhibited the TAPON-LIKE
369 activity toward DDVP at a final concentration of 1.0 mM L^{-1}. PON1, whether it is
370 derived from rabbit serum or human serum, its catalytic activity was dependent on
371 Ca^{2+} ion. In addition, the stability of human PON1 was also dependent on Ca^{2+} ion,
372 which corresponds to the two Ca^{2+} active centers in the three-dimensional structure
373 of PON1 (3). Some ions (such as Zn^{2+}, Co^{2+}, Mn^{2+}, Sr^{2+}, Ba^{2+}, Cd^{2+} or Mg^{2+}) were noted
374 as the protector to keep the human PON in an active form (30). However, the

375 purified reTAPON1-LIKE was more like phosphodiesterase isolated from bacteria
376 *Sphingobium* sp. and *Flavobacterium* sp., which could recovery the activity by
377 obtaining these metal ions (Zn^{2+} , Mn^{2+} , Ba^{2+} , Cd^{2+} or Mg^{2+}). Moreover, (31)
378 reported the hydrolysis of tetriso by an enzyme derived from *Pseudomonas diminuta*
379 as a model for the detoxication of O-ethyl S-(2-diisopropylaminoethyl)
380 methylphosphono; and (32) demonstrated the structure of a novel
381 phosphotriesterase from *Sphingobium* sp. TCM1, which had a familiar binuclear
382 metal center embedded in a seven-bladed β-propeller protein fold. Thus, calcium ion
383 plays an important role in the catalytic activity of reTAPON1-LIKE3 to DDVP, but Ca^{2+},
384 Zn^{2+}, Na^{+} and Ba^{2+} also serves to stabilize the enzyme by keeping its native molecular
385 structure and reactivate the catalytic activity.
386
387 **Discussion**
388
389 The secrets of how DDVP is degraded by *T. atroviride* T23 and the intra- and
390 extracellular enzymes involved in the DDVP biodegradation are still big challenges.
391 Even though a group of *Trichoderma* spp. strains has been widely applied in
392 bioremediation of chemical pesticide-polluted environments, until now, only a few
393 genes, such *hex1* (10) and *TaPdr2* (11), have been found to play roles in the microbial
394 tolerance to stress.
395
396 PON1s derived from mammals such humans, rabbits, and rats demonstrated the

397 metabolic function of removing organophosphate pesticide residues from blood (33).
398 Degradation of human fresh-frozen plasma containing high levels of HuPON1 was
399 rapid, with the shortest half-life of 17.9 min for DDVP (22). Injection of PON1 into
400 rats with acute organophosphate poisoning can decrease the amount of DDVP that
401 enters the blood, lower the peak concentration, and relieve clinical signs(34).
402
403 Since previous researches have already revealed that serum PON1 is responsible for
404 the degradation of DDVP, we hypothesized that a similar mechanism of DDVP
405 biodegradation also present in *Trichoderma*. In our study, an effective protein,
406 designated TAPON1-LIKE, with biodegradation activity of DDVP, was demonstrated to
407 be a hydrolase. The gene encoding TAPON1-LIKE included a 1317-bp ORF, and the
408 deduced amino acid sequence shared a certain homology with HuPON1, which may
409 also have two calcium-binding sites. Using the ATMT method, mutants were
410 constructed, and the function of the *TaPon1-like* gene in the degradation of DDVP
411 was verified. Expression and purification of recombinant enzyme is a way to
412 understand the properties of TAPON1-LIKE. reTAPON1-LIKE showed broad activity
413 ranges for substrate, temperature, and pH. In addition, stimulating and inhibiting
414 metal ions, optimum electron donors, and kinetic parameters were identified.
415
416 Human cDNA clones revealed that PON1 has two common coding polymorphisms,
417 L55M and Q192R. Some studies have shown that genetic polymorphisms of the
418 PON1 192 site can influence the activity of PON1, which may modify the individual

susceptibility to methylparathion-induced toxicity (effects of PON1 polymorphism on the activity of serous PON in workers exposed to organophosphorus pesticides) and the catalytic efficiency of hydrolysis of paraoxon and chlorpyrifos oxon(35). In our study, the sequencing results for *TaPon1*-like verified that the polymorphism of the TAPON1-LIKE 192 site involved residue Arg192, similar to human PON1, which may determine the high catalytic efficiency.

The recombinant enzyme was also confirmed to have some of PON1 activity in the biodegradation of DDVP. Similarly, the TAPON1-LIKE expressed in *E. coli* showed different activities on a range of substrates, and this result suggested that the *TaPon1*-like gene was involved in the biodegradation of different paraoxon-like pesticides, especially for significantly improving the efficiency of pesticide-oxons such as chlorpyrifos-oxon and mevinphos. It has been clearly shown that paraoxon, chlorpyrifos-oxon, and DDVP can all be hydrolyzed by purified HuPON1; in addition, HuPON1 is able to function on a ranges of substrates, such as phenyl acetate, 4-nitrophenyl acetate, TBBL or dihydrocoumarin, chlorpyrifos, diazinon, sarin, or soman, among others(36). It was further found that reTAPON1-like with a broad substrate spectrum towards three types of catalytic substrate, but the enzyme activities showed some differences in kinetic parameters compared with HuPON1. For example, the reTAPON1-LIKE catalytic efficiency for phenyl acetate and 3,4-Dihydrocoumarinpesticide was 5.10×10^{6} and 4.47×10^{6} , which were lower than HuPON1 (26).

441

442 In conclusion, this study found that *T. atroviride* strain T23 produced TAPON1-LIKE
443 protein with functions in the biodegradation of DDVP. The more valuable of this work
444 were provided a novel clue to comprehensively understanding the degradation
445 mechanism of a series of residual organophosphate pesticides through Trichoderma
446 which has been widely applied as bioremediation approach worldwide. The protein's
447 differential roles in the biodegradation of various organophosphate pesticides and its
448 expression and properties in other Trichoderma species remain under study.

449

450 **Materials and Methods**

451

452 Reagents and media

453

454 Main chemical reagents such as pesticide standards, including DDVP, chlorpyrifos,
455 mevinphos, malaoxon, omethoate, triazophos, and methamidophos, were purchased
456 from Dr. Ehrenstorfer GmbH (Augsburg, Germany). Chlorpyrifos-oxon, p-nitrophenyl
457 acetate, p-nitrophenyl butyrate, phenyl acetate, and 3,4-dihydrocoumarin were
458 purchased from J&K Scientific Ltd. (Beijing, China). Other chemical reagents were
459 purchased from the Sinopharm Chemical Reagent Co. Ltd. (Beijing, China). Difco PDA
460 medium was purchased from Becton Dickinson & Co. (Franklin Lakes, NJ, USA).
461 *N-tert*-Butyldimethylsilyl-*N*-methyltrifluoroacetamide (MTBSTFA) was purchased
462 from Sigma (St. Louis, MO, USA). Burk medium contained (liter^{-1}) 0.2 g K_2HPO_4, 0.8 g

463 KH_2PO_4, 0.2 g $MgSO_4 \bullet 7H_2O$, 0.1 g $CaSO_4 \bullet 2H_2O$, 0.0033 g $Na_2MoO_4 \bullet 2H_2O$, 0.005 g
464 $FeSO_4 \bullet 7H_2O$, 1 g $(NH_4)_2SO_4$, and 1 g glucose, pH 6.0. Luria-Bertani (LB), YEP, CYA, and
465 IM media were prepared as previously described (37).
466
467 Strains, plasmids, and culture conditions
468
469 The strains, plasmids, and primers used in this study are listed in Table 3 and Table 4.
470 The wild-type strain T23 and transformants were maintained in PDA (Difco, Becton
471 Dickinson & Co., USA) at 28 °C until sporulation occurred. *Agrobacterium*
472 *tumefaciens* strains were grown on YEP agar or in YEB broth at 28°C. *Escherichia coli*
473 strains were grown in LB broth or LB agar plates. A knockout plasmid, pC1300qh,
474 containing the hygromycin (hygB) resistance gene ORF, was constructed with a
475 pCAMBIA1300 plasmid backbone in which the 35S promoter was replaced with the
476 trpC promoter (37).
477
478 --Table 3--
479 --Table 4--
480
481 Growth and degradation experiments with fungal strains
482
483 In earlier studies it was observed that fungus played a significant role in reducing
484 organic compound levels through enzymes they produce or mycelial adsorption (38),

485 (39), (40), (41). Thus, it was decided to study the degradation and adsorption
486 performed by strain T23. Agar plugs of strain T23 and *TaPon1*-like mutants were
487 precultivated for 2 days in 300 mL flasks containing 500 mL of PD medium on a rotary
488 shaker (180 rpm) at 28 °C, followed by harvesting of mycelia by filtering these
489 cultures through filter paper. The harvested mycelia were washed three times with
490 sterile distilled water, and then 1 g of wet mycelia was transferred to new flasks
491 containing 50 mL of Burk medium. Mycelia transferred in fresh Burk medium without
492 DDVP was used as a control.
493
494 We examined the degradation and adsorption of two DDVPs by strain T23 under two
495 sets of conditions: (a) at ten time points (0-120 h) with an initial concentration of 300
496 μg mL^{-1} DDVP and (b) different initial concentrations of DDVP (100-500 μg mL^{-1}) at 24
497 h.
498
499 The biomass of strain T23 was determined by measuring by the dry weight of mycelia
500 after vacuum drying at -40 °C for 12 h in an Alpha freeze-dryer (Christ, Osterode,
501 Germany). The DDVP concentration in Burk medium and adsorbate concentration of
502 DDVP were assessed using a GC-2010-FPD Plus (Shimadzu, Japan) according to the
503 methods described by Xiao et al. (42). To quantify the absorption of DDVP by mycelia,
504 the dried mycelia were treated with spray gold and then analyzed by scanning
505 electron microscopy (SEM, NOVA NanoSEM 230, FEI, USA) equipped with energy
506 dispersive spectroscopy (EDS, Aztec X-Max, Oxford Instruments, UK). All treatments

507 consisted of three replicates.

508

509 Homologous cloning of *TaPon1*-like genes in *T. atroviride* T23

510

511 We queried the *T. atroviride* genome v2.0 (IMI 206040) on JGI
512 (https://genome.jgi.doe.gov/Triat2/Triat2.home.html) and used local BLAST to search
513 for genes based on the homology domain of *HuPon1* in the human liver.
514 Subsequently, a homologous gene named *TaPon1*-like (GenBank accession number
515 MH802589) was identified in *T. atroviride*. Strain T23 genomic DNA was used as a
516 template for *TaPon1*-like gene amplification with the primers TaPon1-like-F and
517 TaPon1-like-R. Total RNA of T23 was extracted from frozen powdered mycelia using
518 TRIzol (11), and total cDNA of T23 was synthesized using the PrimeScript RT Reagent
519 kit (TaKaRa, Dalian, China). The *TaPon1*-like ORF was PCR-amplified using the primers
520 TaPon1-like-F and TaPon1-like-R. The PCR product was purified from a gel extraction,
521 ligated into a PMD19-T vector, and then used as a PCR template in the assays
522 described below. The recombinant plasmid was transformed into *E. coli* DH5α
523 competent cells, and the cells were then isolated from the transformants and
524 sequenced.

525

526 Comparison of the deduced amino acid sequences in the genes

527

528 The deduced amino acid sequences of *TaPon1*-like genes were compared with the

529 amino acid sequences of similar genes in other species using PDB database search
530 sequences (http://www.rcsb.org/#Subcategory-search_sequences). Amino acid
531 sequence alignment was conducted using ClustalX (43) and Espript 3.0
532 (http://espript.ibcp.fr/ESPript/ESPript/). The phylogenetic tree was constructed using
533 the neighbor-joining method and the software MEGA 5.0. A bootstrap consensus
534 tree was inferred from 1000 replicates and represents the evolutionary history of the
535 taxa analyzed. Signal peptides were analyzed using the SignalP 4.1 Server
536 (http://www.cbs.dtu.dk/services/SignalP/), and the membrane-spanning domains
537 were calculated using TMHMM v. 2.0 (http://www.cbs.dtu.dk/services/TMHMM/).
538
539 Gene expression analysis
540
541 Gene expression analysis of *TaPon1*-like genes in strain T23 was performed under the
542 two different conditions described above. RNA extraction was performed using the
543 Qiagen RNeasy kit following the manufacturer's protocol (Qiagen, Hilden, Germany).
544 One microgram of total RNA was reverse transcribed in a total volume of 20 µL as
545 described above. Transcript levels were quantified by RT-qPCR using SYBR Green PCR
546 Master Mix (TaKaRa, Dalian, China) and the primer pair
547 TaPon-like-RT-F/TaPon-like-RT-R (Table 2) in a LightCycler® 96 system (Roche, Basel,
548 Switzerland). Relative expression levels for the target gene in relation to those of the
549 *actin* gene using the primers actin-RT-F and actin-RT-R were calculated from the Cq
550 values and the primer amplification efficiencies using a formula described previously

551 (44). Gene expression analysis was performed in three biological replicates, with
552 each based on three technical replicates.
553
554 Identification of DDVP degradation metabolites
555
556 Strain T23 (500 μg mL^{-1}) was inoculated into a 500 mL Erlenmeyer flask containing
557 200 mL of Burk medium, and the culture was cultivated as described above. The
558 metabolites were analyzed by gas chromatography-mass spectrometry (GC-MS).
559 After an incubation period, the mycelia were removed by filtering through filter
560 paper. Then, 2% NaCl and 2 mL of HCl were added; 100 mL of anhydrous ethyl ether
561 was subsequently added (equal to 50% of the total volume), and the sample was
562 mixed for 5 min on a vortex mixer. After the liquid stood for 10 min, the ether layer
563 was collected thrice. The ether fractions were concentrated at 30 °C with a rotary
564 evaporator and dried over anhydrous Na_2SO_4.Remaining aqueous phase was
565 concentrated 100-fold at 30 °C with a rotary evaporator until no liquid was present.
566 One of the moist precipitates was then extracted with two 3 mL portions of acetone.
567 The combined acetone extract was concentrated by a stream of N_2, and 100 μL
568 derivative reagent MTBSTFA was added, and the solutions were mixed and heated
569 for 60 min at 70 °C and were then ready for instrumental analysis
570
571 Qualitative and quantitative analyses were performed on a 7890A gas
572 chromatograph and a 5975C mass spectrometer (Agilent Technologies, Milano, Italy).

573 GC-MS instrumental conditions were similar to those of the assay of
574 organophosphate compounds (OPPs) with the following operating parameters: HP-5
575 GC column (30 m×0.32 mm i.d., 0.50 µm film thickness); temperature program of a
576 60 °C initial temperature (6 min hold), 10 °C min^{-1} ramp to 250 °C, and 15 °C min^{-1}
577 ramp to 280 °C (6 min hold). One microliter of each sample was injected into the
578 GC-MS and analyzed using full scan mode, and the instrument was scanned from 10
579 to 600 amu.
580
581 Construction of knockout and complementation *TaPon1*-like mutants
582
583 To generate *TaPon1*-like knockout transformants, a homologous recombination
584 cassette designated pC1300QH-TaPon1-like (Fig. S2A) was constructed with 928-bp 5'
585 flanking sequences and 896-bp 3' flanking sequences using the primers
586 KO-UP-F/KO-UP-R and KO-DOWN-F/KO-DOWN-R. The cloned flanking sequences
587 were restriction-digested with *Hind*III, *Xba*I, *BamH*I, and *Kpn*I (Thermo Fisher
588 Scientific, Shanghai, China), respectively, and these fragments were gel-purified and
589 ligated to modified plasmid pC1300QH. *Agrobacterium tumefaciens*-mediated
590 transformation (ATMT) was performed as previously described (37, 45) for the
591 generation of *TaPon1*-like knockout and complementation transformants.
592
593 The genomic DNA of T23 and transformants was isolated using a modified
594 cetyltrimethylammonium bromide (CTAB) method (46). To identify the *TaPon1*-like

595 knockout transformants, (a) the *TaPon1*-like knockout was verified by attempting to
596 amplify the *TaPon1*-like gene with the primers TaPon1-like-F and TaPon1-like-R; (b)
597 the T-DNA insertion numbers were determined using the primers T-DNA–F and
598 T-DNA–R; (c) RT-PCR analysis of *TaPon1*-like gene expression using Tapon1-like-RT-F/
599 Tapon1-like-RT-R primers. Finally, Southern blotting (47) using *hygB* as a probe was
600 performed to confirm the knockout transformant.
601
602 The plasmid to complement the *TaPon1*-like knockout was constructed with the
603 promoter, which was amplified using the T23 genome as a template with the primers
604 TaPon1-like-PRO-F and TaPon1-like-PRO-R, the amplified *TaPon1*-like ORF, and the
605 trpC terminator amplified from the vector pSilent-1 (48). We ligated the three
606 PCR-amplified fragments into plasmid pC1300TH digested with *Hind*III and *BamH*I
607 using a Hieff Clone™ Plus One Step Cloning Kit (Yeasen, Shanghai, China) to construct
608 the *TaPon1*-like ORF complementary cassette, designated pC1300TH-TaPon1-like (Fig.
609 S3), and then the ORF complementary cassette inserted into the genome of knockout
610 mutant KO1.
611
612 Similarly, the complementary transformants were identified (a) the fragment of
613 *TaPon1*-like gene fusion of *trp C* terminor using Tapon1-like-F/ Tapon1-like-TER-R
614 primers, (b) the fragment of G418 gene amplified from genomic DNA using G418-F/
615 G418-R primers, (c) amplification of TAPON-LIKE complementation cassette from
616 genomic DNA using Tapon1-like-PRO-F/ Tapon1-like-TER-R primers, and (d) RT-PCR

617 analysis of *TaPon1*-like gene expression using Tapon1-like-RT-F/ Tapon1-like-RT-R
618 primers.
619
620 Protein expression and purification of reTAPON1-LIKE
621
622 The expression plasmid pGEX-4T-1-*TaPon1*-like was constructed via the ligation of a
623 partial gene sequence of the *TaPon1*-like gene that was lacking the 90-bp signal
624 peptide into the corresponding restriction sites of a pGEX-4T-1T plasmid digested by
625 *BamH*I/ *EcoR*I. The ligation was performed according to the Hieff Clone™ Plus One
626 Step Cloning Kit manual. The expression plasmid pGEX-4T-1-*TaPon1*-like was then
627 transformed into *E. coli* Origami B (DE3), and the recombinant purified protein was
628 designated reTAPON1-LIKE.
629
630 The transformant was grown at 37 °C and 200 rpm in 1 mL of LB medium containing
631 ampicillin (50 μg mL^{-1}) until the OD600 reached 0.6, and then the culture was
632 cultivated in 1 L of LB liquid medium and induced with 0.6 mM isopropyl
633 β-D-1-thiogalactopyranoside (IPTG). After screening, the best DDVP degradation by
634 the reTAPON1-LIKE expression strain was determined. The cells were harvested at
635 9000 rpm and 4 °C for 10 min and were then washed with PBS (phosphate buffer
636 solution, 10 mM, pH 8.0). The pellets were suspended in lysis buffer: 0.2 mM
637 phenylmethylsulfonyl fluoride (PMSF), 1 mM DL-dithiothreitol (DTT), 1 mM lysozyme,
638 and 50 mM Tris-HCl. The mixture was sonicated with an ultrasonic cell disruptor

(Jingxin Industrial Development Co., LTD, JY92-IIN, Shanghai, China) at 25 °C with 4- to 6-s cycle pulses for 30 min. The lysate containing the reTAPON1-LIKE fusion protein was centrifuged at 12,000 rpm and 4 °C for 20 min, and the supernatant was filtered through a 0.22-μm filter. The filtrate was loaded onto GST•Bind™ Resin (Novagen, Germany) pre-equilibrated with PBS. A flow rate of approximately 10 column volumes per hour was used. Then, the column was washed with 10 volumes of PBS, and the recombinant protein was eluted with three volumes of PBS containing 10 mM reduced glutathione at 4 °C. The target protein was concentrated, and reduced glutathione was removed. ReTAPON1-LIKE, including cell pellets and purified protein, was boiled for 5 min for denaturation, and its concentration was then estimated by SDS-PAGE.

Degradation of DDVP by purified reTAPON1-LIKE enzyme

The enzyme activity of purified reTAPON1-LIKE toward DDVP was measured for 30 min with 100 μM DDVP in a 50 mM glycine buffer, pH 8.5, containing 2.0 M NaCl and 1.0 mM $CaCl_2$. DDVP and metabolites generated by reTAPON1-LIKE degradation activity in the reaction system were extracted with a 1/2 volume of anhydrous ethyl ether and mixed for 5 min at room temperature. The sample was centrifuged at 12,000 rpm, and the upper supernatant was collected in a 1.5 mL tube. This step was repeated twice, and the samples were then concentrated for GC-MS analysis as described above.

661

662 Substrate specificity of reTAPON1-LIKE and enzyme kinetics

663

664 The activity of HuPON1 can normally be measured using three types of substrates:
665 paraoxon, unphosphorylated aryl esters, and lactones (17)

666

667 The paraoxonase activities of reTAPON1-LIKE were measured with paraoxonase-like
668 pesticides such as DDVP (100-500 µM), chlorpyrifos-oxon (100-500 µM), mevinphos
669 (10-100 µM), malaoxon (10-100 µM), omethoate (100-500 µM), triazophos (100-500
670 µM), and methamidophos (100-500 µM). The reaction conditions included a 50 mM
671 glycine buffer, pH 8.5, containing 2.0 M NaCl and 1.0 mM $CaCl_2$, as previously
672 reported (49). The extraction of these compounds was performed according to the
673 methods described above and detected by GC-FPD.

674

675 The arylesterase activity of reTAPON1-LIKE was determined with phenyl acetate
676 (1.0-5.0 mM), p-nitrophenyl acetate (0.5-2.5 mM), and p-nitrophenyl butyrate
677 (0.25-1.25 mM) as substrates in 20 mM Tris-HCl buffer, pH 8.0, containing 1.0 mM
678 $CaCl_2$, as previously described (50).

679

680 The lactonase activity of reTAPON1-LIKEs was determined with dihydrocoumarin
681 (0.1-2.0 mM) as substrate in 25 mM Tris-HCl buffer, pH 7.4, containing 1.0 mM $CaCl_2$,
682 as previously described (50).

683

684 The arylesterase and lactonase activities of reTAPON1-LIKE were detected using a
685 SpectraMax i3x Multi-Mode Detection Platform (Molecular Devices, CA, USA).
686 Enzyme activities are expressed in international units (U) per liter (L) of supernatant
687 enzyme reTAPON1-LIKE, and one unit is defined as the amount of enzyme that
688 catalyzes the turnover of 1 μM of substrate per min at 25 °C.

689

690 The catalytic constants k_{cat} and K_m were determined under standard assay conditions
691 with 7 different concentrations of various substrates and a range of reTAPON1-LIKE
692 concentrations (0.05-5.00 μM). Kinetic parameters were determined using a
693 Lineweaver-Burk plot.

694

695 Biochemical properties of purified reTAPON1-LIKE

696

697 The most desirable pH was determined by incubating the purified enzyme in
698 phosphate buffer (pH 5.0-8.0), glycine-NaOH (pH 9.0-11.0), and Tris-HCl buffer (pH
699 7.5-9.0). To study the effect of temperature on the activity of purified reTAPON1-LIKE
700 against DDVP at pH 8.0, the temperature of the assays was varied from 25 °C to 70 °C.
701 Enzyme activity was reported as a percentage of the highest value, which was set as
702 100%.

703

704 The effects of metal ions and inhibitors on enzyme activity were investigated at 25 °C

and pH 8.0. The purified reTAPON1-LIKE was incubated with 1 mM solutions of the metal salts $MgCl_2$, $MnCl_2$, $ZnCl_2$, $CaCl_2$, $CuCl_2$, $BaCl_2$, $FeCl_3$, and NaCl for 10 min to determine residual activity. The results were expressed as percentages, and the values of the native enzyme without metal ion addition were set as 100%.

Acknowledgements

This study was supported by the following projects: The National Key Research and Development Program of China (2017YFD0200403, 2017YFD0201108), the Natural Science Foundation of China (31672072; 31750110455), the Intergovernmental Key International Scientific and Technological Innovation Cooperation (2017YFE0104900), the 948 Project of the Ministry of Agriculture (2016-X48), and CARS-02. We all appreciate Lurong Xu for guiding us in the operation of the GC-MS instrument and analyzing the data.

References

1. Gan Q, Singh RM, Wu T, Jans U. 2006. Kinetics and mechanism of degradation of dichlorvos in aqueous solutions containing reduced sulfur species. Environmental Science & Technology 40:5717-5723.

2. Liu C, Qiang Z, Adams C, Tian F, Zhang T. 2009. Kinetics and mechanism for degradation of dichlorvos by permanganate in drinking water treatment. Water Res

727 43:3435-42.

728 3. Lynch SM, Lorenz J, Klotz S. 2014. Inclusion of calcium during isolation of
729 high-density lipoprotein from plasma maintains antioxidant function. Analytical
730 Biochemistry 454:41-43.

731 4. Ren Z, Zhang X, Wang X, Qi P, Zhang B, Zeng Y, Fu R, Miao M. 2015. AChE
732 inhibition: One dominant factor for swimming behavior changes of Daphnia magna
733 under DDVP exposure. Chemosphere 120:252-257.

734 5. Evgenidou E, Konstantinou I, Fytianos K, Albanis T. 2006. Study of the removal of
735 dichlorvos and dimethoate in a titanium dioxide mediated photocatalytic process
736 through the examination of intermediates and the reaction mechanism. J Hazard
737 Mater 137:1056-64.

738 6. Singh BK. 2008. Organophosphorus-degrading bacteria: ecology and industrial
739 applications. Nature Reviews Microbiology 7:156-164.

740 7. Zhang X-H, Zhang G-S, Zhang Z-H, Xu J-H, Li S-P. 2006. Isolation and
741 Characterization of a Dichlorvos-Degrading Strain DDV-1 of Ochrobactrum sp.
742 Pedosphere 16:64-71.

743 8. Harman GE, Howell CR, Viterbo A, Chet I, Lorito M. 2004. Trichoderma species -
744 Opportunistic, avirulent plant symbionts. Nature Reviews Microbiology 2:43-56.

745 9. Zhang GZ, Zhang XJ, Hong-Mei LI, Guo K, Yang HT. 2016. Isolation and
746 Characterization of the Chlorpyrifos-degrading Trichoderma Strains from the
747 Vegetable Soil in Greenhouse. Biotechnology Bulletin.

748 10. Tang J, Li Y, Fu K, Yuan X, Gao S, Wu Q, Yu C, Shi W, Chen J. 2014. Disruption of

hex1 in Trichoderma atroviride leads to loss of Woronin body and decreased tolerance to dichlorvos. Biotechnology Letters 36:751-759.

11. Zhang T, Tang J, Sun J, Yu C, Liu Z, Chen J. 2015. Hex1-related transcriptome of Trichoderma atroviride reveals expression patterns of ABC transporters associated with tolerance to dichlorvos. Biotechnol Lett 37:1421-9.

12. Jacquet P, Daude D, Bzdrenga J, Masson P, Elias M, Chabriere E. 2016. Current and emerging strategies for organophosphate decontamination: special focus on hyperstable enzymes. Environmental Science and Pollution Research 23:8200-8218.

13. Draganov DI, La Du BN. 2004. Pharmacogenetics of paraoxonases: a brief review. Naunyn Schmiedebergs Arch Pharmacol 369:78-88.

14. Draganov DI. 2010. Lactonases with oragnophosphatase activity: Structural and evolutionary perspectives. Chemico-Biological Interactions 187:370-372.

15. Anonymous. !!! INVALID CITATION !!!

16. Sun W, Chen Y, Liu L, Tang J, Chen J, Liu P. 2010. Conidia immobilization of T-DNA inserted Trichoderma atroviride mutant AMT-28 with dichlorvos degradation ability and exploration of biodegradation mechanism. Bioresource Technology 101:9197-9203.

17. Ceron JJ, Tecles F, Tvarijonaviciute A. 2014. Serum paraoxonase 1 (PON1) measurement: an update. Bmc Veterinary Research 10.

18. Li WF, Costa LG, Furlong CE. 1993. Serum paraoxonase status: a major factor in determining resistance to organophosphates. J Toxicol Environ Health 40:337-46.

19. Teiber JF, Draganov DI, La Du BN. 2003. Lactonase and lactonizing activities of

771 human serum paraoxonase (PON1) and rabbit serum PON3. Biochemical
772 Pharmacology 66:887-896.
773 20. Bustos N, Cruz-Alcalde A, Iriel A, Fernandez Cirelli A, Sans C. 2018. Sunlight and
774 UVC-254 irradiation induced photodegradation of organophosphorus pesticide
775 dichlorvos in aqueous matrices. Sci Total Environ 649:592-600.
776 21. Costa LG, McDonald BE, Murphy SD, Omenn GS, Richter RJ, Motulsky AG, Furlong
777 CE. 1990. Serum paraoxonase and its influence on paraoxon and chlorpyrifos-oxon
778 toxicity in rats. Toxicology and Applied Pharmacology 103:66-76.
779 22. von der Wellen J, Bierwisch A, Worek F, Thiermann H, Wille T. 2016. Kinetics of
780 pesticide degradation by human fresh frozen plasma (FFP) in vitro. Toxicology Letters
781 244:124-128.
782 23. Aharoni A, Gaidukov L, Yagur S, Toker L, Silman I, Tawfik DS. 2004. Directed
783 evolution of mammalian paraoxonases PON1 and PON3 for bacterial expression and
784 catalytic specialization. Proceedings of the National Academy of Sciences of the
785 United States of America 101:482-487.
786 24. Suzuki SM, Stevens RC, Richter RJ, Cole TB, Park S, Otto TC, Cerasoli DM, Lenz DE,
787 Furlong CE. 2010. Engineering Human PON1 in an E. coli Expression System, p
788 37-45. *In* Reddy ST (ed), Paraoxonases in Inflammation, Infection, and Toxicology, vol
789 660. Springer-Verlag Berlin, Berlin.
790 25. Furlong CE, Costa LG, Hassett C, Richter RJ, Sundstrom JA, Adler DA, Disteche CM,
791 Omiecinski CJ, Chapline C, Crabb JW, Humbert R. 1993. Human and rabbit
792 paraoxonases: Purification, cloning, sequencing, mapping and role of polymorphism in

793 organophosphate detoxification. Chemico-Biological Interactions 87:35-48.

794 26. Furlong CE, Cole TB, Jarvik GP, Pettan-Brewer C, Geiss GK, Richter RJ, Shih DM,
795 Tward AD, Lusis AJ, Costa LG. 2005. Role of Paraoxonase (PON1) Status in
796 Pesticide Sensitivity: Genetic and Temporal Determinants. NeuroToxicology
797 26:651-659.

798 27. Furlong CE, Suzuki SM, Stevens RC, Marsillach J, Richter RJ, Jarvik GP, Checkoway
799 H, Samii A, Costa LG, Griffith A, Roberts JW, Yearout D, Zabetian CP. 2010. Human
800 PON1, a biomarker of risk of disease and exposure. Chemico-Biological Interactions
801 187:355-361.

802 28. Richter RJ, Jarvik GP, Furlong CE. 2009. Paraoxonase 1 (PON1) status and substrate
803 hydrolysis. Toxicology and Applied Pharmacology 235:1-9.

804 29. Worth J. 2002. Paraoxonase polymorphisms and organophosphates. The Lancet
805 360:802-803.

806 30. Kanamori-Kataoka M, Seto Y. 2009. Paraoxonase activity against nerve gases
807 measured by capillary electrophoresis and characterization of human serum
808 paraoxonase (PON1) polymorphism in the coding region (Q192R). Analytical
809 Biochemistry 385:94-100.

810 31. Hoskin FCG, Walker JE, Dettbarn WD, Wild JR. 1995. Hydrolysis of tetriso by an
811 enzyme derived from pseudomonas-diminuta as a model for the detoxication of
812 o-ethyl s-(2-diisopropylaminoethyl) methylphosphonothiolate(VX). Biochemical
813 Pharmacology 49:711-715.

814 32. Mabanglo MF, Xiang DF, Bigley AN, Raushel FM. 2016. Structure of a Novel

815 Phosphotriesterase from Sphingobium sp TCM1: A Familiar Binuclear Metal Center
816 Embedded in a Seven-Bladed beta-Propeller Protein Fold. Biochemistry
817 55:3963-3974.
818 33. Valiyaveettil M, Alamneh Y, Biggemann L, Soojhawon I, Farag HA, Agrawal P, Doctor
819 BP, Nambiar MP. 2011. In vitro efficacy of paraoxonase 1 from multiple sources
820 against various organophosphates. Toxicology in Vitro 25:905-913.
821 34. Wang NN, Yuan L, Dai H, Han ZK, Zhao M. 2011. Effect of PON1 on dichlorvos
822 toxicokinetics. Emergency Medicine Journal Emj 28:313-315.
823 35. Furlong CE, Cole TB, Walter BJ, Shih DM, Tward A, Lusis AJ, Timchalk C, Richter RJ,
824 Costa LG. 2005. Paraoxonase 1 (PON1) status and risk of insecticide exposure.
825 Journal of Biochemical and Molecular Toxicology 19:182-183.
826 36. Ruggerone B, Bonelli F, Nocera I, Paltrinieri S, Giordano A, Sgorbini M. 2018.
827 Validation of a paraoxon-based method for measurement of paraoxonase (PON-1)
828 activity and establishment of RIs in horses. Veterinary Clinical Pathology 47:69-77.
829 37. Kunitake E, Tani S, Sumitani J-i, Kawaguchi T. 2011. Agrobacterium
830 tumefaciens-mediated transformation of Aspergillus aculeatus for insertional
831 mutagenesis. Amb Express 1.
832 38. Maqbool Z, Hussain S, Imran M, Mahmood F, Shahzad T, Ahmed Z, Azeem F,
833 Muzammil S. 2016. Perspectives of using fungi as bioresource for bioremediation of
834 pesticides in the environment: a critical review. Environ Sci Pollut Res Int
835 23:16904-25.
836 39. Collado IG, Aleu J, Pinedo-Rivilla C. 2009. Pollutants Biodegradation by Fungi.

837 Current Organic Chemistry 13:-.

838 40. Kaushik G, Thakur IS. 2009. Isolation of fungi and optimization of process parameters
839 for decolorization of distillery mill effluent. World Journal of Microbiology &
840 Biotechnology 25:955-964.

841 41. Kaushik G, Gopal M, Thakur IS. 2010. Evaluation of performance and community
842 dynamics of microorganisms during treatment of distillery spent wash in a three stage
843 bioreactor. Bioresource Technology 101:4296-4305.

844 42. Xiao Q, Hu B, Yu C, Xia L, Jiang Z. 2006. Optimization of a single-drop
845 microextraction procedure for the determination of organophosphorus pesticides in
846 water and fruit juice with gas chromatography-flame photometric detection. Talanta
847 69:848-855.

848 43. Thompson JD, Gibson TJ, Plewniak F, Jeanmougin F, Higgins DG. 1997. The
849 CLUSTAL_X windows interface: flexible strategies for multiple sequence alignment
850 aided by quality analysis tools. Nucleic Acids Research 25:4876-4882.

851 44. Pfaffl MW, Hageleit M. 2001. Validities of mRNA quantification using recombinant
852 RNA and recombinant DNA external calibration curves in real-time RT-PCR.
853 Biotechnology Letters 23:275-282.

854 45. Fu K, Fan L, Li Y, Gao S, Chen J. 2012. Tmac1, a transcription factor which regulated
855 high affinity copper transport in Trichoderma reesei. Microbiol Res 167:536-43.

856 46. Agbagwa IO, Datta S, Patil PG, Singh P, Nadarajan N. 2012. A protocol for
857 high-quality genomic DNA extraction from legumes. Genetics and Molecular Research
858 11:4632-4639.

859 47. Yu C, Fan L, Wu Q, Fu K, Gao S, Wang M, Gao J, Li Y, Chen J. 2014. Biological role
860 of Trichoderma harzianum-derived platelet-activating factor acetylhydrolase (PAF-AH)
861 on stress response and antagonism. PLoS One 9:e100367.
862 48. Nakayashiki H, Hanada S, Quoc NB, Kadotani N, Tosa Y, Mayama S. 2005. RNA
863 silencing as a tool for exploring gene function in ascomycete fungi. Fungal Genetics
864 and Biology 42:275-283.
865 49. Amitai G, Gaidukov L, Adani R, Yishay S, Yacov G, Kushnir M, Teitlboim S,
866 Lindenbaum M, Bel P, Khersonsky O, Tawfik DS, Meshulam H. 2006. Enhanced
867 stereoselective hydrolysis of toxic organophosphates by directly evolved variants of
868 mammalian serum paraoxonase. Febs Journal 273:1906-1919.
869 50. Bhattacharyya T, Nicholls SJ, Topol EJ, Zhang RL, Yang X, Schmitt D, Fu XM, Shao
870 MY, Brennan DM, Ellis SG, Brennan ML, Allayee H, Lusis AJ, Hazen SL. 2008.
871 Relationship of paraoxonase 1 (PON1) gene polymorphisms and functional activity
872 with systemic oxidative stress and cardiovascular risk. Jama-Journal of the American
873 Medical Association 299:1265-1276.

874

875 **Table captions**

876

877 Table 1 Kinetic analysis of substrate hydrolysis by the reTAPON1-LIKE enzyme

878 Table 2 Effects of different metal ions on the activity of the reTAPON1-LIKE enzyme

879 Table 3 Strains and plasmids used in this study

880 Table 4 Primers used in this study

881

882 **Figure Legends**

883

884 Fig. 1. Fungal growth and DDVP degradation rate in cultures of *T. atroviride* T23. (A)
885 Effects of DDVP concentration on fungal biomass (column) and DDVP degradation
886 rate (solid square). DDVP was added at the beginning of the cultures. The biomass
887 and DDVP degradation were determined after 24 h of incubation. (B) Effect of
888 incubation time on fungal biomass. DDVP at 300 μg mL^{-1} was added at the beginning
889 of the cultures. The group without DDVP was used as a control. Solid square, control;
890 solid circle, under 300 μg mL^{-1} DDVP. Each value is expressed as the means ± standard
891 errors of three replicates.

892

893 Fig. 2. Gas chromatogram and mass spectrum detection of DDVP degradation by
894 strain T23. A gas chromatogram of the extract obtained from the culture at 5 days
895 treated with the MTBSTFA (A) and non-treated (B). The black line indicated strain T23
896 incubate in Burk medium with initial concentration of 300 μg mL^{-1} DDVP and the red
897 line indicated strain T23 incubate in Burk medium. Potential catabolic pathway for
898 DDVP degradation by strain T23 (C). Mass spectra of DDVP (E) degradation products
899 formed the *tert*-butyldimethylsilyl derivatives were identified of the peak with RTs of
900 13.075 min (D), 14.115 min (F) and 21.83min (G). Mass spectra of DDVP (E)
901 degradation products were identified of the peak with RTs of 5.577 min (H) and
902 10.606min (I).

903

904 Fig. 3. Expression analyses of *TaPon1*-like in *T. atroviride* T23. (A) *TaPon1*-like gene
905 expression in liquid Burk medium with different concentrations of DDVP (100-500 µg
906 mL^{-1}) at 24 h. Medium without DDVP was used as a control. The graph shows the
907 averages and means ± standard errors of three replicates. (B) Time course of
908 *TaPon1*-like expression at 300 µg mL^{-1} DDVP. Time points on the *x-axis* represent the
909 duration of DDVP stress. Relative mRNA levels were normalized according to *actin*
910 gene expression and were calculated using the $2^{-\triangle\triangle Ct}$ method.

911

912 Fig. 4. Phylogenetic tree of TAPON1-LIKE and related paraoxonases, arylesterases,
913 and hydrolases constructed using the neighbor-joining method. The hydrolases and
914 their accession numbers: HuPON1 (P27169), MosPON1 (P52430), RabPON1
915 (P27170), RatPON1 (P55159), BdOPD (P0A434), SsARE (B5BLW5), BdOPD (P0A434),
916 SfOPD (P0A433), MosPON2 (Q91090), HuPON3 (Q15166), RabPON3 (Q9BGN0), and
917 RatPON3 (Q68FP2).

918

919 Fig. 5. Multiple alignments of amino acid sequences of TAPON1-LIKE and similar
920 proteins. The deduced amino acid sequences of human PON1, human PON2, human
921 PON3, OPD (*Brevundimonas diminuta*), and TAPON1-LIKE are shown, respectively,
922 from the first line to the bottom line. For the human species, there are two
923 polymorphic sites that are indicated above at positions 55 and 192. Three yellow,
924 boxed regions represent potential calcium-binding regions; the arrows represent

925 conserved amino acid residues.

926

927 Fig. 6. Degradation rate of DDVP by T23 and *TaPon1-like* mutants. Degradation rate
928 curves of DDVP by mycelia of T23 and *TaPon1-like* mutants. The initial concentration
929 of DDVP was 300 μg mL^{-1}. CK, Burk medium with DDVP only; T23, wild type strain;
930 CO1, *TaPon1-like* complementation mutant; KO1, *TaPon1-like* knockout mutant. Data
931 are expressed as the means±standard errors of three replicates.

932

933 Fig. 7. SDS-PAGE analysis of reTAPON1-LIKE heterologs expressed in the *E. coli*
934 recombinant system.Lane M: protein marker, lane 1: supernatant protein of *E. coli*
935 Origami B(DE3) harboring reTAPON1-LIKE induced by IPTG, lane 2: purification of
936 reTAPON1-LIKE, with a predicted molecular mass of approximately 71 kDa.

937

938 Fig. 8. Effects of pH (A) and temperature (B) on reTAPON1-LIKE enzymatic activity.
939 DDVP was used as the substrate. Activity at the optimal pH and temperature was
940 defined as 100%. Data are expressed as the means ± standard errors of three
941 replicates.

Table captions

Table 1 Kinetic analysis of substrate hydrolysis by the reTAPON1-LIKE enzyme

Substrate	K_m (mM)	k_{cat} s^{-1}	Catalytic efficiency (k_{cat}/K_m s^{-1} M^{-1})
Dichlorvos	0.23±0.02	204.3±2.0	8.88×10^5
Chlorpyrifos-oxon	0.32±0.05	1936.0±51.6	6.05×10^6
Mevinphos	0.44±0.04	6.5±0.3	1.47×10^4
Malaoxon	0.72±0.01	9.7±0.4	1.35×10^4
Omethoate	0.79±0.12	6.1±0.1	7.72×10^3
Methamidophos	nd	nd	nd
Chlorpyrifos	nd	nd	nd
Triazophos	nd	nd	nd
Phenyl acetate	0.89±0.06	4535.2±22.6	5.10×10^6
p-Nitrophenyl acetate	1.12±0.14	211.4±10.9	1.98×10^5
p-Nitrophenyl butyrate	1.58±0.12	59.8±1.1	3.78×10^4
3,4-Dihydrocoumarin	0.73±0.01	3261.1±73.0	4.47×10^6

Note: Each value corresponds to the average of three different determinations. nd, not determined.

Table 2 Effects of different metal ions on the activity of the reTAPON1-LIKE enzyme

Additive	Concentration (mM)	Relative activity (%)
No addition		100±1.5
Metal ions		
Ca^{2+}	1	589.7±3.3
Zn^{2+}	1	234.4±5.6
Mg^{2+}	1	121.2±4.6
Cu^{2+}	1	<5
Ni^{2+}	1	95.5±2.4
Na^{+}	1	176.5±5.2
Ba^{2+}	1	151.6±1.4
Mn^{2+}	1	119.9±0.8
Fe^{2+}	1	93.2±0.6
Co^{2+}	1	82.7±1.8
Enzyme inhibitors		
EDTA	1	nd

Note: The activities of metal ion-treated reTAPON1-LIKE enzyme were assayed under standard assay conditions after incubation with 1 mM of various metal ions. The activity of the reTAPON1-LIKE enzyme with no added metal ions was set as 100%. Each value corresponds to the average of three different determinations.

Table 3 Strains and plasmids used in this study

Strain or plasmid	Description [a]	Reference or source
Strains		
T. atroviride T23	Wild-type DDVP degrader	Laboratory stock
T. atroviride KO1	Derivative of strainT23, site-directed knockout mutant of *TaPon1*-like ORF cassette, Hyg^r	This study
T. atroviride CO1	Derivative of KO 5, complementation transformant of *TaPon1*-like ORF cassette, G418^r	This study
A. tumefaciens AGL1	Host strain for *Agrobacterium tumefaciens*-mediated transformation of filamentous fungi, Rif^r	Laboratory stock
E. coli DH5α	Host strain for cloning vectors	TaKaRa
E. coli Origami B (DE3)	Host strain for expression vector	Novagen
Plasmids		
pGEX-4T-1	Expression vector; Amp^r	Novagen
pGEX-4T-1-*TaPon11*-like	pGEX-4T-1 harboring the *TaPon1*-like gene with signal peptide deleted	This study
pMD19-T	T-A cloning vector, Amp^r	TaKaRa
pSilent-1	Vector including trpC promoter and terminator sequences, Amp^r	Laboratory stock
pC1300QH	Knockout broad-host-range shuttle vector, Kan^r	(46)
pC1300QH-*TaPon11*-like	pC1300QH harboring the 5′ flanking fragment and 3′ flanking fragment of the gene *TaPon*-like, Kan^r	This study
pC1300TH	Complementation broad-host-range shuttle vector, Kan^r	(46)
pC1300TH-TaPon1-like	pC1300TH harboring the *TaPon*-like ORF complementation cassette, Kan^r	This study

[a] Amp^r, ampicillin resistant; Kan^r, kanamycin resistant; Rif, rifampin resistant; Hyg^r, hygromycin B; G418^r, geneticin resistant.

Table 4 Primers used in this study

Overexpression-purification	Nucleotide sequence(5'-3')[a]
TaPon1-like-F	**CG**GGATCCATGGCGGCCCGCGCCTCAAT
TaPon1-like-R	**G**GAATTCTCACAAATCGATCTTGACAG
Reverse transcription	
Tapon1-like-RT-F	TCACCACGCCAAACGACATA
TaPon1-like-RT-R	CAACTGACGCATGGACTCCT
actin-RT-F	CGACTGCTCTCCAACAAGC
actin-RT-R	TTCACTCAGGCTCACAAAGC
Gene knockout	
KO-UP-F	**CCC**AAGCTTATTCGCGATTCCAGCCTATG
KO-UP-R	**GC**TCTAGACGTGACGAATACGCAAGCAC
KO-DOWN-F	**CG**GGATCCATTGCGGTGATCAGAAGGGG
KO-DOWN-R	**GG**GGTACCTCACAATGCCACACCACAGT
HYG-F	GCTCTCGGAGGGCGAAGAAT
HYG-R	GCCTGCGCGACGGACGCACTG
T-DNA -F	CTGGAAGCTCATGTGTCGGT
T-DNA-R	TGCGGCCATTGTCCGTCAGG
Mutant complementation	
TaPon1-like-PRO-F	AAACGACGGCCAGTGCCAAGCTTTTAGCTCAAAGCCCAGAAGCA
TaPon1-like-PRO-R	TGATTGAGGCGCGGGCCGCCATCGTGACGAATACGCAAGCAC
TaPon1-like-TER-F	TTGCTGTCAAGATCGATTTGATGGTGAGCAAGGGCGAGGA
TaPon1-like-TER-R	GAGCTCGGTACCCGGGGATCCAACCCAGGGGCTGGTGACGG
G418-F	GTTGTCACTGAAGCGGGAAGG
G418-R	CGATACCGTAAAGCACGAGGAA
Heterologous expression of the TaPon-like	
TaPon1-like-GST-DELECT- SignalP-F	GATCTGGTTCCGCGTGGATCCATGGGCGCCTTTCGACAGCCA
TaPon1-like-GST-R	CTCGAGTCGACCCGGGAATTCCAAATCGATCTTGACAGCAAT

[a] Restriction recognition sequences are underlined, and enhancer sequences are in boldface type.

A

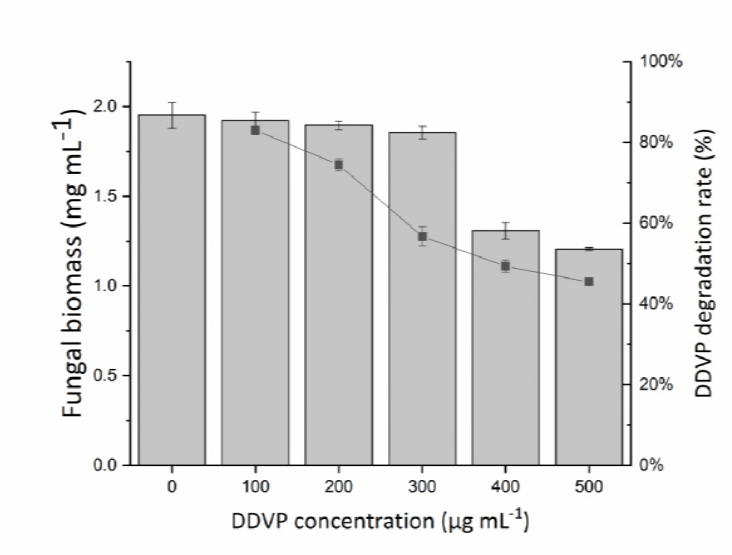

B

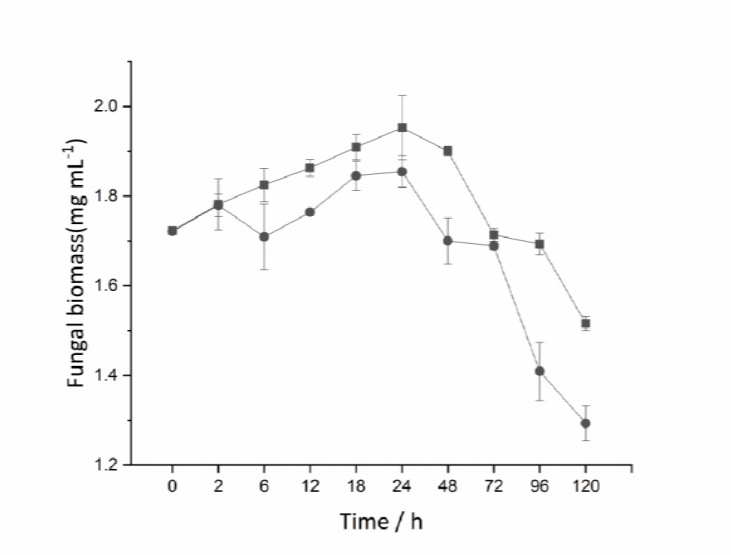

Fig. 1 Fungal growth and DDVP degradation rate in cultures of *T. atroviride* T23. (A) Effects of DDVP concentration on fungal biomass (column) and DDVP degradation rate (solid square). DDVP was added at the beginning of the cultures. The biomass and DDVP degradation were determined after 24 h of incubation. (B) Effect of incubation time on fungal biomass. DDVP at 300 μg mL^{-1} was added at the beginning of the cultures. The group without DDVP was used as a control. Solid square, control; solid circle, under 300 μg mL^{-1} DDVP. Each value are expressed as the means ± standard errors of three replicates.

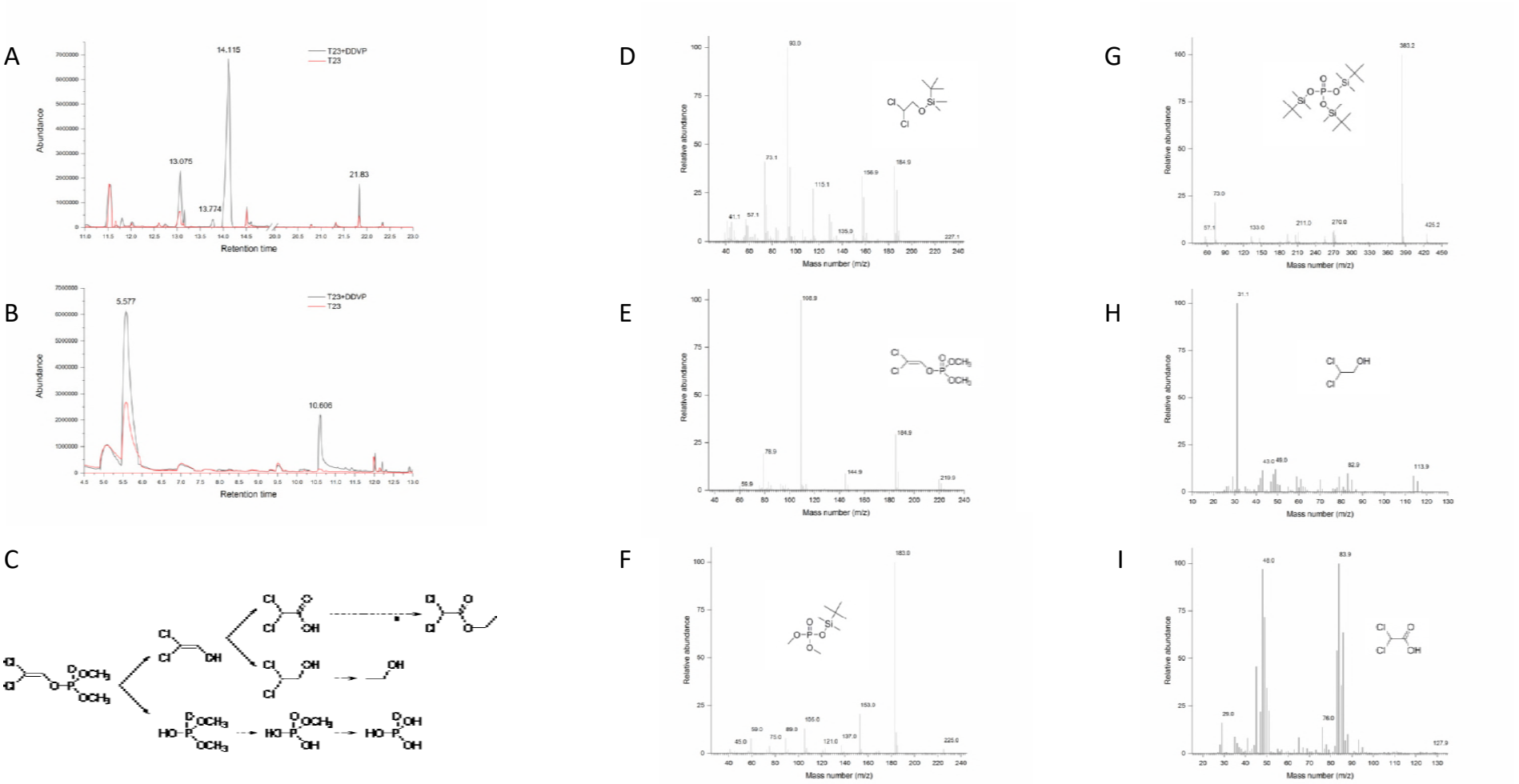

Fig. 2 Gas chromatogram and mass spectrum detection of DDVP degradation by strain T23. A gas chromatogram of the extract obtained from the culture at 5 days treated with the MTBSTFA (A) and non treated (B). The black line indicated strain T23 incubate in Burk medium with initial concentration of 300 μg mL^{-1} DDVP and the red line indicated strain T23 incubate in Burk medium. Potential catabolic pathway for DDVP degradation by strain T23 (C). Mass spectra of DDVP (E) degradation products formed the *tert*-butyldimethylsilyl derivatives were identified of the peak with RTs of 13.075 min (D), 14.115 min (F) and 21.83min (G). Mass spectra of DDVP (E) degradation products were identified of the peak with RTs of 5.577 min (H) and 10.606min (I).

A

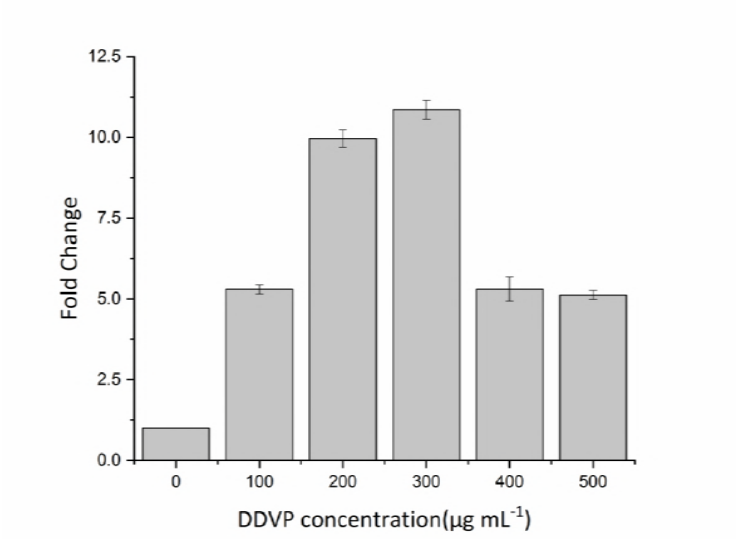

B

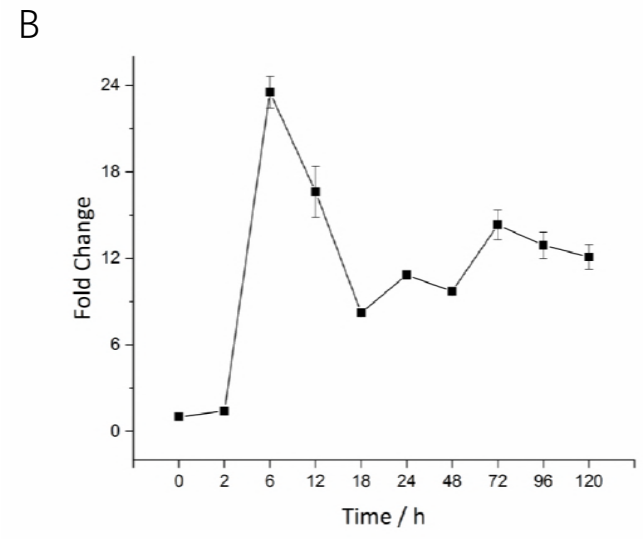

Fig. 3 Expression analyses of *TaPon1*-like in *T. atroviride* strain T23. (A) *TaPon1*-like gene expression in liquid Burk medium with different concentrations of DDVP (100-500 μg mL^{-1}) at 24 h. Medium without DDVP was used as a control. The graph shows the averages and means ± standard errors of three replicates. (B) Time course of *TaPon1*-like expression at 300 μg mL^{-1} DDVP. Time points on the *x-axis* represent the duration of DDVP stress. Relative mRNA levels were normalized according to *actin* gene expression and were calculated using the $2^{-\Delta\Delta Ct}$ method. Data are expressed as the means ± standard errors of three replicates.

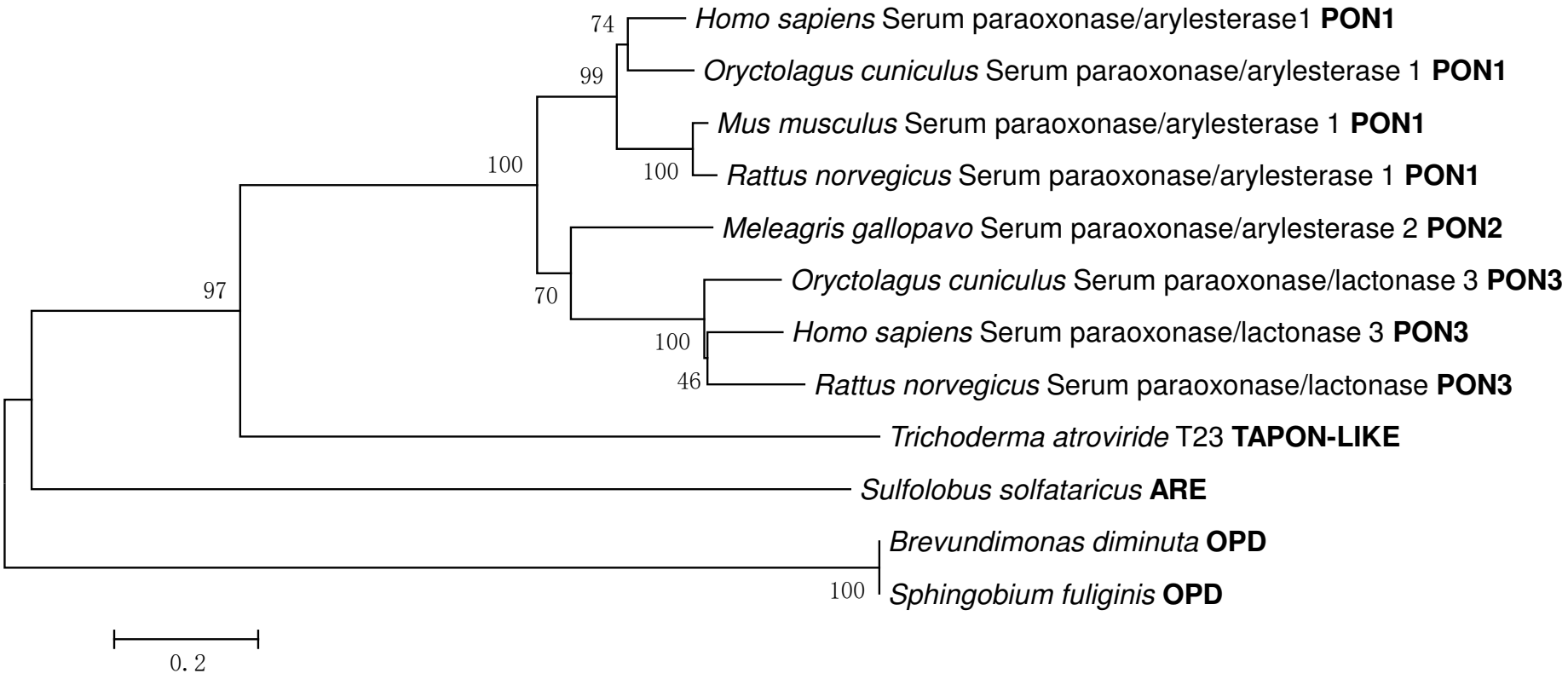

Fig. 4 Phylogenetic tree of TAPON1-LIKE and related paraoxonases, arylesterases, and hydrolases constructed using the neighbor-joining method. The hydrolases and their accession numbers: HuPON1 (P27169), MosPON1 (P52430), RabPON1 (P27170), RatPON1 (P55159), BdOPD (P0A434), SsARE (B5BLW5), BdOPD (P0A434), SfOPD (P0A433), MosPON2 (Q91090), HuPON3 (Q15166), RabPON3 (Q9BGN0), and RatPON3 (Q68FP2).

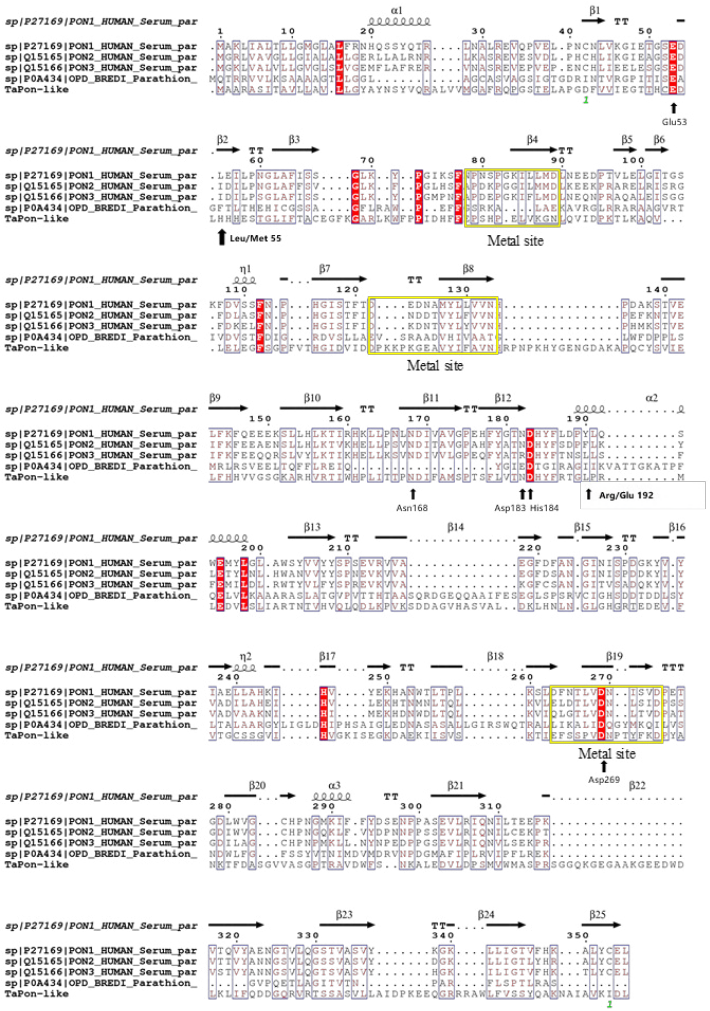

Fig. 5 Multiple alignments of amino acid sequences of TAPON1-LIKE and similar proteins .
The deduced amino acid sequences of human PON1, human PON2, human PON3, OPD (*Brevundimonas diminuta*), and TAPON1-LIKE are shown, respectively, from the first line to the bottom line. For the human species, there are two polymorphic sites that are indicated above at positions 55 and 192. Three yellow, boxed regions represent potential calcium-binding regions; the arrows represent conserved amino acid residues.

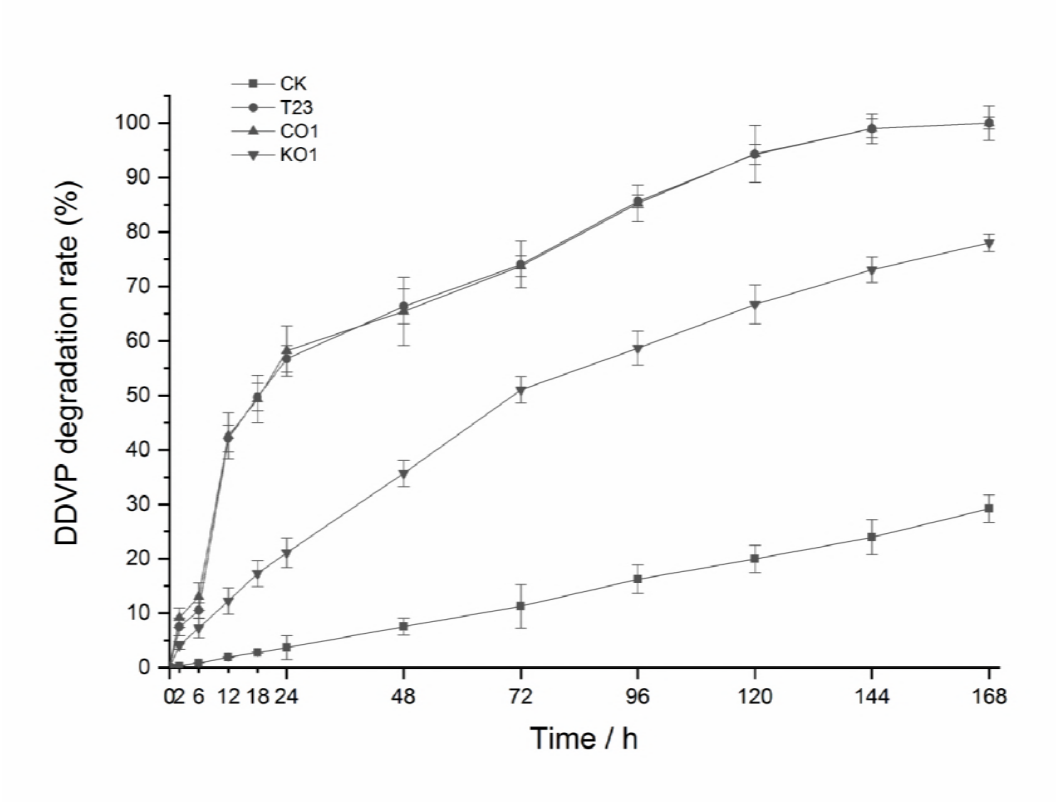

Fig. 6 Degradation rate of DDVP by T23 and *TaPon1-like* mutants. Degradation rate curves of DDVP by mycelia of T23 and *TaPon1-like* mutants. The initial concentration of DDVP was 300 μg mL^{-1}. CK, Burk medium with DDVP only; T23, wild type strain; CO1, *TaPon1-like* complementation mutant; KO1, *TaPon1-like* knockout mutant. Data are expressed as the means ± standard errors of three replicates.

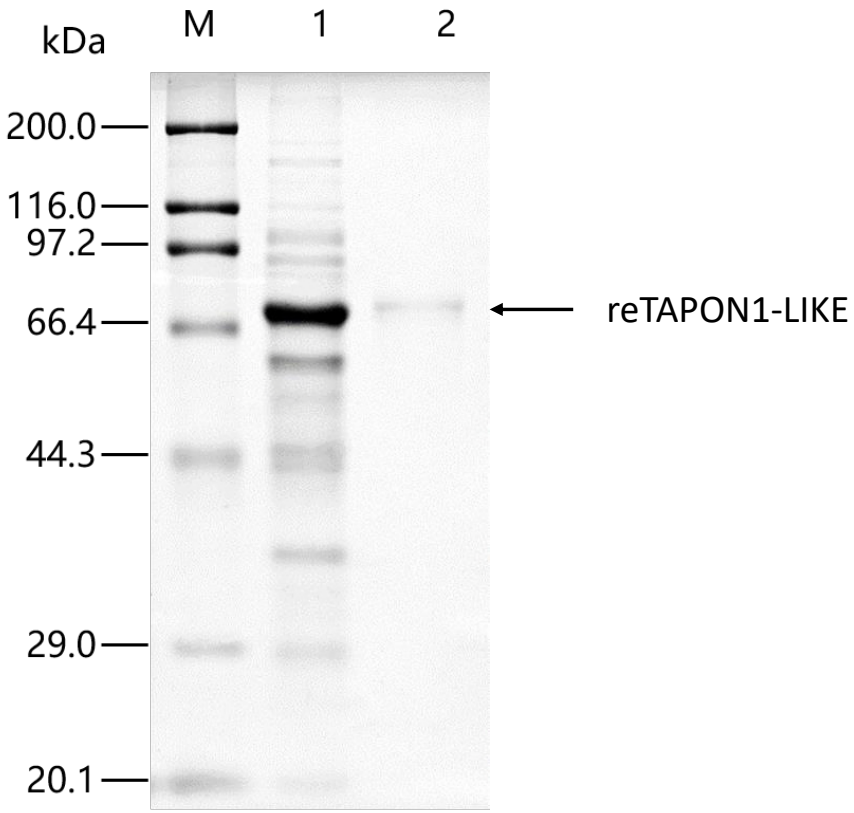

Fig. 7 SDS-PAGE analysis of reTAPON1-LIKE heterologs expressed in the *E. coli* recombinant system
Lane M: protein marker, lane 1: supernatant protein of *E. coli* Origami B(DE3) harboring reTAPON1-LIKE induced by IPTG, lane 2: purification of reTAPON1-LIKE, with a predicted molecular mass of approximately 71 kDa.

A

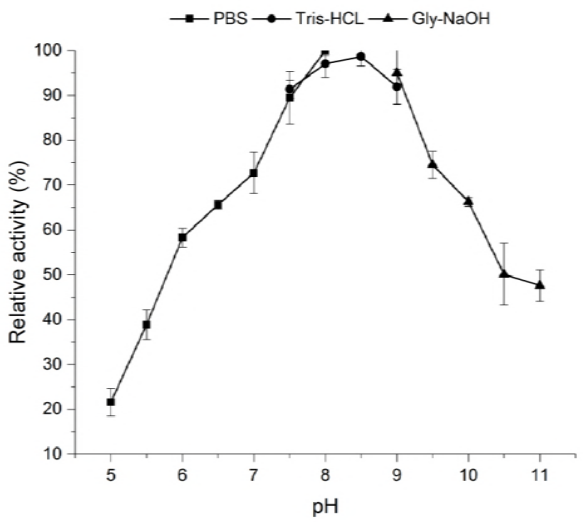

B

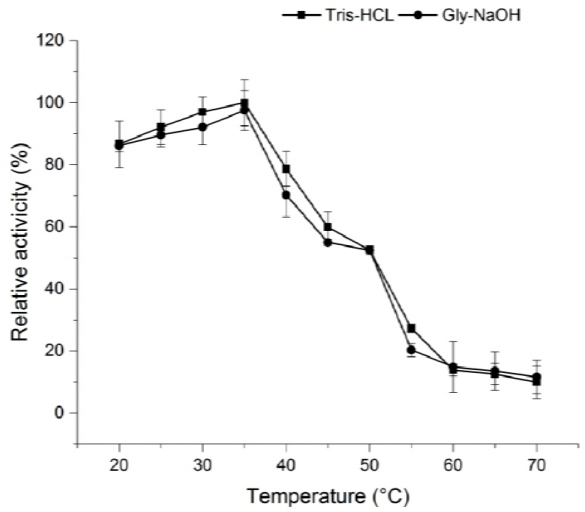

Fig. 8 Effects of pH (A) and temperature (B) on reTAPON1-LIKE enzymatic activity. DDVP was used as the substrate. Activity at the optimal pH and temperature was defined as 100%. Data are expressed as the means ± standard errors of three replicates.